Mixing Flow Characteristics in a Vessel Agitated by the Screw Impeller With a Draught Tube

Yeng-Yung Tsui[1]
Professor
e-mail: yytsui@mail.nctu.edu.tw

Yu-Chang Hu
Graduate Student

Department of Mechanical Engineering,
National Chiao Tung University,
Hsinchu 300, Taiwan

The circulating flow in a vessel induced by rotating impellers has drawn a lot of interests in industries for mixing different fluids. It used to rely on experiments to correlate the performance with system parameters because of the theoretical difficulty to analyze such a complex flow. The recent development of computational methods makes it possible to obtain the entire flow field via solving the Navier–Stokes equations. In this study, a computational procedure, based on multiple frames of reference and unstructured grid methodology, was used to investigate the flow in a vessel stirred by a screw impeller rotating in a draught tube. The performance of the mixer was characterized by circulation number, power number, and nondimensionalized mixing energy. The effects on these dimensionless parameters were examined by varying the settings of tank diameter, shaft diameter, screw pitch, and the clearance between the impeller and the draught tube. Also investigated was the flow system without the draught tube. The flow mechanisms to cause these effects were delineated in detail. [DOI: 10.1115/1.2903815]

1 Introduction

The process of fluid mixing is commonly used in industries. To blend different fluids, a vessel is equipped with a rotational impeller. A swirling flow, i.e., a flow rotating about the vessel axis, is generated by the impeller. The function of the impeller is to ensure transport of a fluid element to anywhere in the tank. In order to fulfill this objective, axial vortices, i.e., loop flows circulating from the top region of the tank to the bottom region, must be induced. Thus, the flow in the tank is inevitably three dimensional. The contact surfaces between different fluids are then deformed by the three-dimensional flow. Since different fluid materials are mixed in the interface layer via molecular diffusion, the deformed and, thus, elongated contact surface leads to the enhancement of fluid mixing.

For low-viscosity fluids, the most commonly used impellers are the disk-type flat blade turbines and the pitched-blade turbines [1]. The low viscosity of the fluids and the smaller size, compared with the tank, render the turbine impellers suitable for high-speed rotation, which makes the flow field turbulent. Turbulent flows are helpful in fluid mixing because the contact surfaces between different fluids are greatly wrinkled by the turbulence fluctuations. At higher viscosities, these impellers lose their effectiveness due to the difficulty to achieve high shear conditions because large power consumption is demanded. Instead, helical ribbon impellers or screw impellers, rotating at low speeds, are preferred.

The screw impeller, despite its small diameter, produces significant secondary circulation when incorporating a draught tube and is the main concern of the present study. This mixer works in a similar manner to the screw extruder. However, the former functions to maximize pumping flow with a low pressure increase, whereas the latter works to maximize pressure rise with a low pumping capacity. In the past, most analyses of the pumping flow in the screw mixer are based on an analogy to the extruder. As seen in Refs. [2,3], the flow in a tube pumped by a screw can be mainly divided into a drag flow q_d and a pressure flow q_p,

$$q = q_d - q_p \tag{1}$$

The drag flow q_d resulting from the relative motion between the screw and the casing is a forward flow in the positive direction of the axis. It was treated as a fully developed flow between two parallel plates with one plate moving at the rotational speed to drive the fluid flow, which is similar to the well-known Couette flow. When the screw pump operates, pressures builds up in the pump, resulting in a high pressure at the outlet. The adverse pressure gradient brings about a back flow in the negative direction of the axis. This pressure flow q_p can be analyzed by assuming a Poiseuille flow between the plates.

The above simple models were also used to estimate power requirements. The power consumed by the drag flow is obtained via calculating the internal heat generation due to viscous dissipation. Both the flows in the channel direction and in the transverse direction need to be taken into consideration in estimating the energy dissipation. For the pressure flow, the power required is the power expended as flow energy in raising the pressure of the fluid, which is equal to the product of the pressure rise in the screw pump and the maximum pumping flow rate corresponding to zero pressure gradients.

For the pressure flow, the pressure rise between the inlet and the outlet of the screw pump needs to be known. In general, the pressure rise is determined from experiments. However, Sykora [4] used the frictional loss in the flow through the annular span between the draught tube and the tank to estimate this pressure rise. To account for the effects of the side walls and the curvature of the flow channel in the pump at low helical angles, shape factors were introduced [2,3].

In the past, most studies were done to correlate three key characteristic parameters (power number, mixing time, and circulation number) to geometric parameters, such as the tank diameter, the length of the screw, the pitch of the impeller, and the width of the impeller blade [4–10]. These correlations were expressed in dimensionless form to generalize their applicability. When geometric configurations are fixed, the dependence of the three characteristic parameters on the rotational speed of the screw impeller (n) or the Reynolds number (Re) can be summarized for Newtonian fluids as

$$N_P \,\mathrm{Re} = \mathrm{const} \tag{2}$$

[1]Corresponding author.

Contributed by the Fluids Engineering Division of ASME for publication in the JOURNAL OF FLUIDS ENGINEERING. Manuscript received January 31, 2007; final manuscript received October 18, 2007; published online April 3, 2008. Assoc. Editor:r Yu-Tai Lee.

$$N_Q = \text{const} \tag{3}$$

$$\tau_m n = \text{const} \tag{4}$$

where N_P is the power number, N_Q the circulation number, and τ_m the mixing time. These relationships are valid for $\text{Re} < 20$. For higher Reynolds numbers, the results of Carreau et al. [11] revealed that mixing time gradually decreases with Reynolds number. They also found that

$$\frac{N_p \text{Re}}{N_Q} = \text{const} \tag{5}$$

The circulation number increases from the value at low Reynolds numbers with increasing Re to eventually attain another constant value. It was concluded by them that the ratio of the mixing time to the circulation time (the time for the flow to complete a circulation loop in the vessel) is a constant.

In view of the above review, despite the fruitful achievement in relating the screw mixer performance to the system configuration settings, details about the flow field were not delineated in these experimental works and the simple analytical models cannot portray the flow field precisely. Mathematical methods, which solve the Navier–Stokes equations, give complete pictures of velocity and pressure fields and are thus useful to analyze the flow. Although they have already been widely employed in industrial applications, their use in simulating the screw mixer is very limited. As far as we are aware, only Kuncewicz et al. [12] adopted a numerical method to study the effects of the tank diameter and the pitch of the screw impeller on the mixer performance. In their simulations, the flow field was simplified by assuming it to be two dimensional. The action of the rotating impeller on the flow is realized by imposing a form drag force and a frictional drag force onto the momentum equations [13]. Two empirical coefficients, characterizing the two forces, need to be specified. Recently, the present authors developed a three-dimensional computational method, which is based on a fully conservative finite volume method and incorporates unstructured grid techniques. Multiple frames of reference were employed to tackle the rotation of the impeller. This method had been successfully used in the simulation of the vacuum pump of the Holweck type [14] and the mixer with pitched-blade turbines [15]. In this study, it is employed to examine the effects of various geometric parameters on the screw mixer with a draught tube.

2 Mathematical Method

A schematic sketch of an agitated system with a screw impeller together with a draught tube is shown in Fig. 1. For numerical calculations, the draught tube is divided into an inner part and an outer part. The outer part covers the clearance region between the impeller blade and the inner wall of the tube. In this clearance region and the bulk region outside the draught tube, the frame of reference is stationary. A rotational frame is imposed on the inner part of the tube to allow the blade of the impeller to sweep across this region. The flow field in the agitated vessel is assumed to be quasisteady, implying that the screw impeller is frozen at a specific position. The governing equations in the rotational frame can then be cast into the following form:

$$\frac{\partial[(U_j^* - U_{gj}^*)]}{\partial x_j^*} = 0 \tag{6}$$

$$\frac{\partial[(U_j^* - U_{gj}^*)(U_i^* - U_{gi}^*)]}{\partial x_j^*} = -\frac{\partial p^*}{\partial x_i^*} + \frac{1}{\text{Re}} \frac{\partial}{\partial x_j^*} \left(\frac{\partial (U_i^* - U_{gi}^*)}{\partial x_j^*} \right) - \varepsilon_{mni} \Omega_m U_{gn}^* - 2\varepsilon_{mni} \Omega_m (U_n^* - U_{gn}^*) \tag{7}$$

The above equations are expressed in dimensionless form in which the coordinates, velocities, and pressure are normalized as

$$x_j^* = \frac{x_j}{d}, \quad U_j^* = \frac{U_j}{nd}, \quad p^* = \frac{p}{\rho n^2 d^2} \tag{8}$$

where d is the diameter of the impeller, n the rotational frequency, and ρ the density of the fluid. The Reynolds number Re is defined as $\rho n d^2/\mu$, where μ is the molecular viscosity of the fluid. $U_j^* - U_{gj}^*$ represents the flow velocity with respect to the moving grid and $U_{gj}^* = \varepsilon_{jpq} \Omega_p x_q^*$ is the velocity of the moving grid rotating with the impeller. $\Omega_j (= 2\pi n e_j)$ is the angular velocity of the impeller. The effects of the rotational frame are represented by the body forces given in the last two terms in the momentum equation, corresponding to the centrifugal force and the Coriolis force. In the stationary frame of reference, the grid velocity $U_{gj}^* = 0$ and the body forces are dropped.

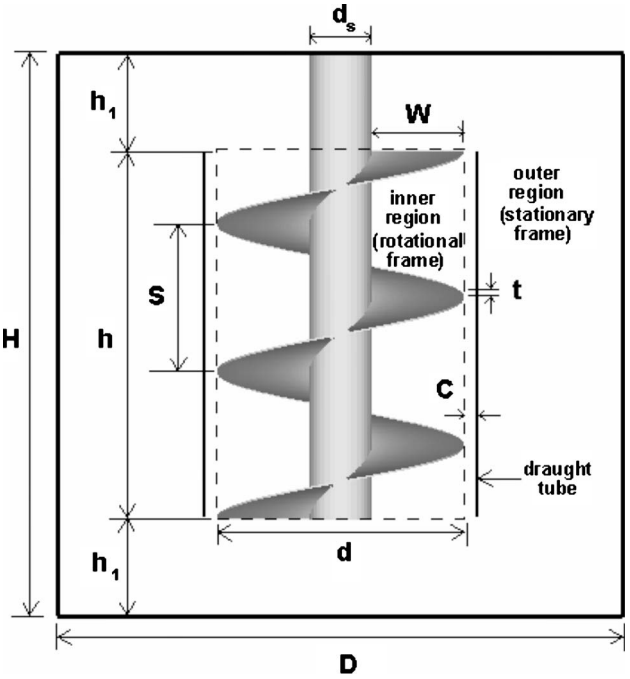

Fig. 1 A sketch of the mixing system

There is a need to have a comprehensive tool to handle various flow configurations encountered in industries. To meet this requirement, the authors have developed a general code in recent years such that the flow with irregular boundaries can be analyzed. The analytic tool is based on a fully conservative finite volume method applicable to unstructured grids, which are made of polyhedrons with arbitrary geometric topology. This method is briefly described in the following.

The transport equations are first integrated over a control volume which, in principle, can be of arbitrary geometry. With the aid of the divergence theorem, the volume integrals of the convection and diffusion terms are transformed into surface integrals. It is followed by the use of midpoint rule to yield discretization form

$$\sum_f [(\vec{U} - \vec{U}_g)_f \cdot \vec{s}_f] \phi_f = \sum_f \frac{1}{\text{Re}} \nabla \phi_f \cdot \vec{s}_f + q \Delta v \tag{9}$$

where the subscript f denotes the face values, $\vec{s}_f$ is the surface vector of the considered face, and ϕ represents the components of the relative velocity $(\vec{U} - \vec{U}_g)$. The last term in the equation represents all the terms apart from the convection and diffusion terms. The summation is taken over all the faces of the control surface.

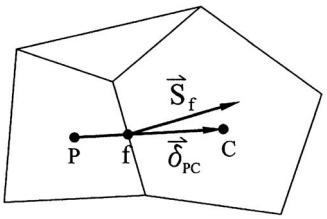

Fig. 2 Illustration of a principal node and a neighboring node with a common face

The convective value ϕ_f through each face is approximated by a high-order scheme,

$$\phi_f = \phi^{\mathrm{UD}} + \gamma(\nabla\phi)^{\mathrm{UD}} \cdot \vec{\delta} \tag{10}$$

where the superscript UD denotes the value evaluated at a node upstream of the face under consideration and $\vec{\delta}$ is the distance vector directed from the upwind node to the centroid of the face. In the equation, γ is a blending factor falling in the range between 0 and 1. For a value of 0, it simply degenerates into the upwind difference scheme. For $\gamma=1$, the scheme is second order accurate. In the present calculations, a value of 0.9 is assigned to γ.

The diffusive flux is further modeled by the following approximation:

$$\frac{1}{\mathrm{Re}} \nabla \phi_f \cdot \vec{s}_f = \frac{1}{\mathrm{Re}} \frac{s_f^2}{\vec{\delta}_{PC} \cdot \vec{s}_f} (\phi_C - \phi_P) + \frac{1}{\mathrm{Re}} \overline{\nabla \phi_f} \cdot \left(\vec{s}_f - \frac{s_f^2}{\vec{\delta}_{PC} \cdot \vec{s}_f} \vec{\delta}_{PC} \right) \tag{11}$$

where (see Fig. 2) the subscripts P and C denote the principal and the neighboring nodes sharing a common face f, and $\vec{\delta}_{PC}$ is a distance vector connecting these two nodes. The face gradient $\overline{\nabla \phi_f}$ is obtained via interpolation from the gradients at the two nodes.

In solving the discretized transport equations, the first terms on the right-hand side in Eqs. (10) and (11) are implicitly treated, while the second terms in the equations are tackled in an explicit manner using the deferred-correction procedure. It also needs to be noted that the computational molecules for the nodes in one frame immediately adjacent to the interface between the two reference frames include nodal points in the other frame. To correctly evaluate the momentum flux transported through the interface, the velocities at these neighboring nodes must be transformed onto the frame where the considered node is located.

After solving momentum equations, the resulting velocities must be adjusted, and the prevailing pressure must be upgraded in a way that the continuity equation is satisfied. The enforcement of conservation of mass results in a pressure-correction equation. The discretized momentum equations and the pressure-correction equation are sequentially solved in an iterative manner. Iterations are performed to account for the nonlinearities, the coupling between velocities and pressure, and the deferred-correction terms mentioned above. More details about the method can be found in Refs. [14,16].

3 Results and Discussion

A drawing of the mixing system with a screw-in-a-tube agitator is given in Fig. 1. A benchmark configuration of the mixing system has a screw impeller with diameter $d=126$ mm and length $h=1.5d$. The diameter D and the height H of the agitated tank are $D=H=2.3d$. The screw impeller has a shaft of diameter $d_S=0.254d$ and a clearance $C=0.05d$. The pitch of the screw impeller is $S=0.6d$. The width of the screw blade W is equal to $(d-d_S)/2$, and the distances between the impeller and both the top and the bottom of the tank are $h_1=(H-h)/2$. The impeller rotates at a speed of 59 rpm, which is equivalent to a Reynolds number of 1.52.

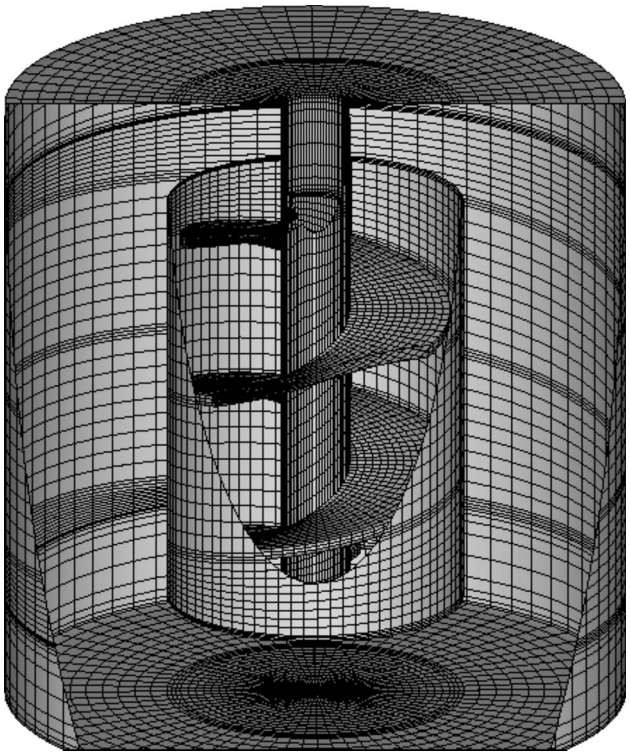

Fig. 3 A computational mesh

To generate unstructured grids, the computational domain is first divided into 80 blocks. In each block, an algebraic method is used to create a suitable grid. After the grids for all the blocks are constructed, the grid nodes are readdressed. An example of the resulting mesh is presented in Fig. 3. To examine grid effects on the mixing flow performance, grids with about 120,000, 200,000, 300,000, and 380,000 cells have been tested. It was found that the power number (defined by Eq. (14)) gradually increases with the cell number from 287 to 301.6. However, the difference between the two finest grids is only 0.4%. The circulation number (defined by Eq. (12)) is less sensitive to the choice of grid. It varies from 0.196 for the coarsest grid to 0.193 for the other grids. In the following, the grid with about 380,000 cells is adopted for calculations. The no-slip conditions are imposed on all the surfaces of the system. The flow in the vessel is assumed to be motionless as the initial condition.

The flow field, illustrated in Fig. 4, shows that fluid is drawn by the rotating impeller into the draught tube from the upper opening and emerges from the bottom end, followed by an upward flow outside the tube to complete a circulation loop. To validate the methodology, calculations have been conducted to compare with the measurements of Seichter et al. [8] and Seichter [9]. In the experiments, the liquids to be mixed were solutions of starch syrup in water, which exhibit a Newtonian behavior. The flow velocities were measured using a thermal resistor. To measure the torque, the mixing vessel was placed on a turntable. The torque produced by the rotating impeller was transmitted to a silon thread and compensated on a desk balance. There are two major differences between the experiments and the simulations. One is that the thickness of the impeller is not given in the experiments. Therefore, a guessed value for the thickness was used in simulations. The other is the upper surface of the flow in the vessel, which is open to air. However, it is assumed to be a solid wall in calculations. A comparison of the axial velocity in the annular

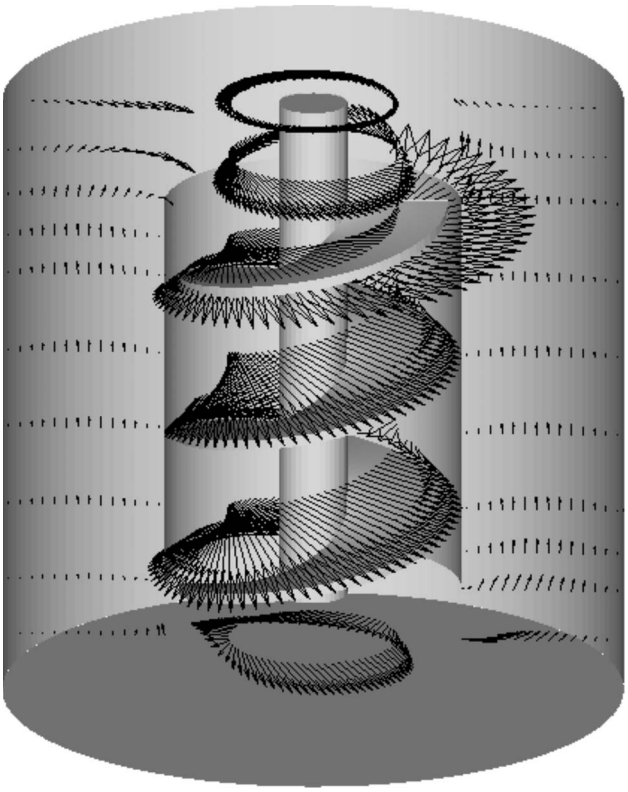

Fig. 4 Typical flow field

region outside the tube at the midheight plane is shown in Fig. 5. Three rotational speeds, corresponding to Re=0.92, 1.26, and 1.52, were under consideration. Since the thickness of the impeller blade was not clear, three values, corresponding to $t=1$ mm, 5 mm, and 8 mm, were chosen to test its effects. It is obvious from the figures that the larger the blade thickness, the lower the flow rate. Both the experiments and the predictions indicate that the flow in the annulus approaches a fully developed state with the velocity close to a parabolic profile. A further comparison between predictions and measurements for Re=1.52 is given in Table 1 in which the circulation number N_Q and the power number N_P^* are shown. The corresponding N_Q and N_P^* for Re=1.26 and 0.92 are

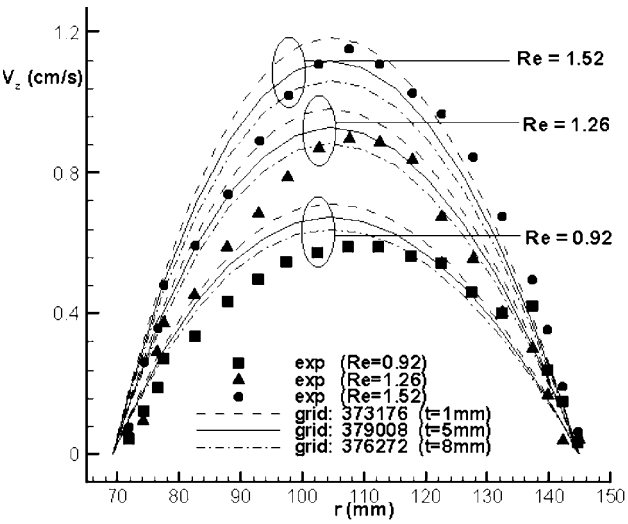

Fig. 5 Comparison of predicted and measured axial velocities in the annular region outside the tube

Table 1 Comparison between predicted and measured circulation numbers and power numbers for different blade thicknesses

	$t=1$ mm	$t=5$ mm	$t=8$ mm	Expt.
N_Q	0.204	0.193	0.183	0.178
N_P^*	242.6	301.6	341.6	306.1

almost the same as the values listed in Table 1 due to the fact these numbers are independent of the Reynolds number, as seen from Eqs. (2) and (3). For the largest thickness case, the predicted N_Q is close to the experimental data, but the predicted N_P^* is too high. For $t=5$ mm, the predicted N_P^* is in good agreement with the measurements and the predicted N_Q is only about 8% higher. Therefore, 5 mm of blade thickness, being about 4% of the impeller diameter, is used throughout the following results.

The performance of the mixer is characterized in terms of three dimensionless parameters: circulation number N_Q, power number N_P^*, and energy of mixing E.

The circulation number is defined by

$$N_Q = \frac{Q}{nd^3} \tag{12}$$

Here, Q is the volumetric flow rate through the draught tube. It is exactly the same as the flow rate in the annulus outside the tube due to mass conservation.

The power number is usually given as

$$N_P = \frac{P}{\rho n^3 d^5} \tag{13}$$

where P is the power consumed by the impeller. The power required to drive the impeller can be divided into two parts: one due to the pressure force acting on the impeller blade and the other due to the frictional force acting on the surfaces of the blade and the shaft. This power number is a function of Reynolds number. Another form of the power number can be expressed by

$$N_P^* = \frac{P}{\mu n^2 d^3} \tag{14}$$

These two expressions are related by

$$N_P^* = N_P \,\mathrm{Re} \tag{15}$$

As seen from Eq. (2), N_P^* is a constant for low Reynolds numbers.

A criterion to evaluate the effectiveness of the mixer is the energy of mixing E nondimensionalized as [12]

$$E = \frac{P\tau_m}{\mu n d^3} \tag{16}$$

where τ_m is the time needed for the mixing process to reach a homogenization state. To estimate the mixing time, unsteady flow simulations must be undertaken, which require large computational time. Alternatively, we can use the circulation time instead of the mixing time because it was observed that the time required for mixing is proportional to the time required for circulation [11]. The circulation time is given by

$$\tau_c = \frac{\Delta V}{Q} \tag{17}$$

where ΔV is the volume of the considered tank. By substituting $4\tau_c$ into Eq. (16) to replace τ_m [11], we can redefine E as

$$E = \pi \frac{N_P^*}{N_Q} \left(\frac{H}{D}\right) \left(\frac{D}{d}\right)^3 \tag{18}$$

It is noted that in the equation, N_P^*/N_Q represents the power required per unit of circulating flow. It can be used as an indicator for pumping effectiveness [15] but is not suitable for mixing effectiveness because the geometric size of the tank needs to be taken into account in the mixing process.

3.1 Effects of Tank Diameter. To examine the influence of the relative size of the stirred tank to the impeller, the diameter of the tank is gradually enlarged, while those of both the screw impeller and the draught tube remain unchanged. Its effects on the pumping capacity, power consumption, and mixing effectiveness are illustrated in Figs. 6(*a*)–6(*c*). In the figures, two sets of calculations corresponding to cases with a constant impeller shaft ($d_s/d=0.254$, where d is fixed) and a variable shaft ($d_s/D=0.11$) are presented. In the constant shaft case, the pump configuration is fixed, while the pump shaft diameter d_s will be increased with the enlarged tank in the variable shaft case. The inclusion of the latter is simply used to compare with the experiments of Seichter et al. [8] and the predictions of Kuncewicz et al. [12] because there are no data available for the former case for comparison. Considering the case with a fixed shaft, for small values of D close to d, the circulating flow rate N_Q is small because of the great frictional resistance of the narrow passage between the draught tube and the tank wall. The flow rate quickly builds up when the annular space is enlarged to $D/d=2.3$, followed by leveling off to a value of $N_Q=0.35$. Theoretically, the power number N_P^* is maximized as the tank diameter is reduced to the tube diameter because a very high pressure gradient is generated, but without any fluid flow. When the tank diameter is increased, the power requirement decreases sharply and then N_P^* reaches nearly a constant value of 225 after D becomes larger than $2.3d$. Also shown in Fig. 6(*b*) are the two parts of power number due to the pressure force ($N_{P,p}^*$) and the frictional force ($N_{P,f}^*$). For small tank diameters, $N_{P,p}^*$ quickly decreases and $N_{P,f}^*$ gradually increases. Both are attributed to the release of the flow in the annular region as D/d increases. At large diameters, power consumption is mainly attributed to the frictional loss, which is about three times the pressure loss. Figure 6(*c*) illustrates that the energy required for mixing is reduced first and then quickly increases when the tank is enlarged. There exists a minimum point at $D/d=2$. This value is smaller than the value of 2.3 at which the circulating flow rate becomes nearly a maximum and the power consumption a minimum. The results can be understood in view of Eq. (18) in which the mixing energy is proportional to D^3.

For the variable shaft case with $d_s/D=0.11$, the flow channel in the draught tube is narrowed as the shaft diameter increases with the enlarged tank, resulting in a reduction in N_Q and an increase in N_P^* when D is greater than $2.3d$. A similar trend for N_Q can be found in the results of Kuncewicz et al. [12]. However, the power number N_P^* increases with increasing D in the present calculations for D greater than $2.3d$ but continues to decrease in the calculations of Kuncewicz et al. It will be shown in Sec. 3.2 that an increase in shaft diameter will cause an increase in frictional force on the shaft surface, which leads to a large frictional loss. Therefore, the predictions of Kuncewicz et al. are not reliable. The cause of the decreasing behavior is thought to be due to their calculation procedure. As mentioned in the Introduction, in their two-dimensional calculations, two drag coefficients need to be specified to account for the action forces by the impeller. These coefficients were determined by some pilot tests to fit the experimental data and then used throughout the rest of the calculations. It is conjectured that these coefficients may require adjustment for the cases with large D/d. This may explain why their results have a good agreement with the measurements at low values of D/d.

The experimental data of Seichter et al. [8] are also included in the figures. There exist some differences between the present predications and the measurements. It needs to be emphasized that

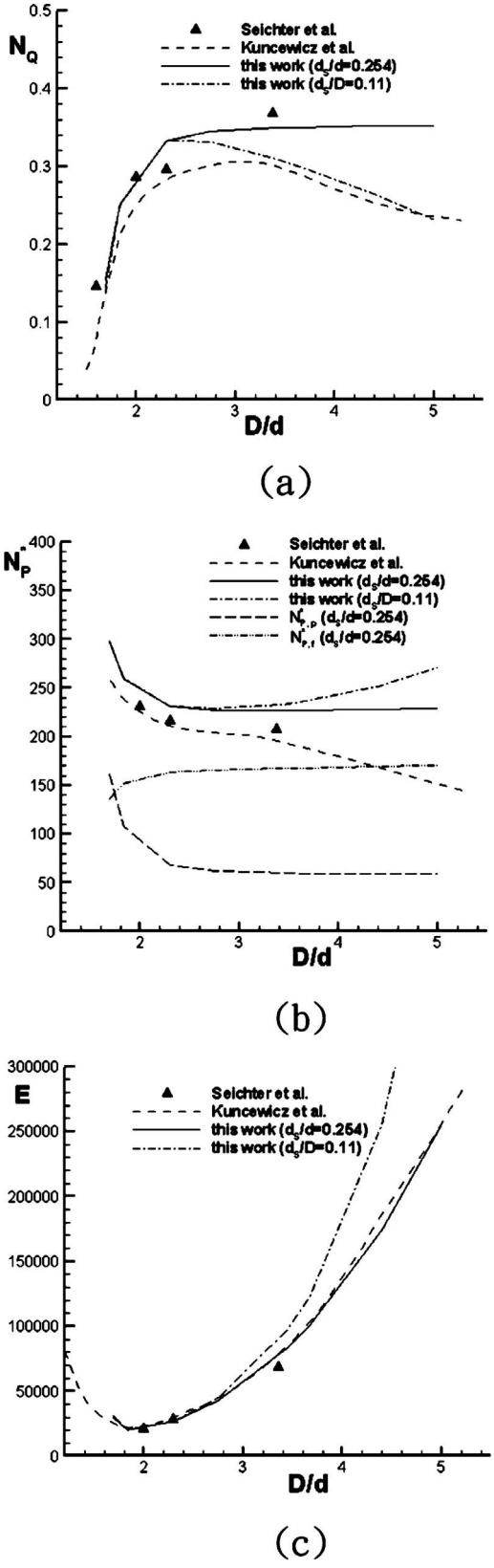

Fig. 6 Variation of (*a*) circulation number, (*b*) power number, and (*c*) mixing energy against tank diameter *D*

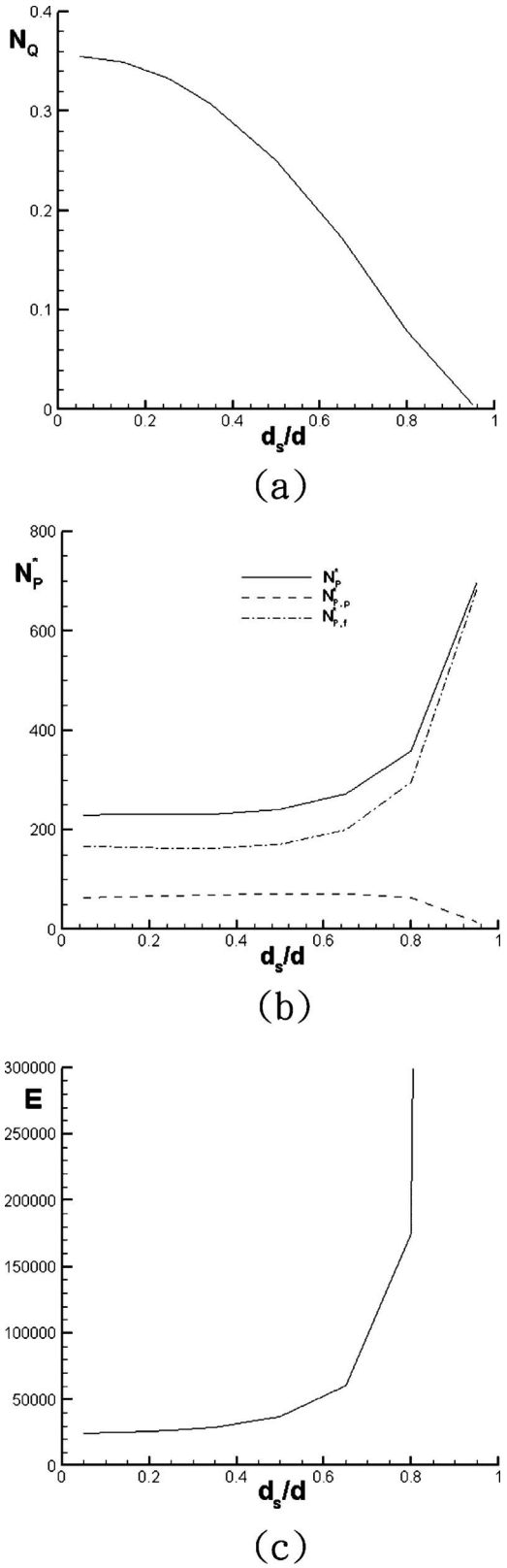

Fig. 7 Variation of (*a*) circulation number, (*b*) power number, and (*c*) mixing energy against shaft diameter d_s

the simulation cannot completely mimic the experiments. As discussed above, the thickness of the impeller blade and that of the draught tube were not clear in the experiments.

3.2 Effects of Shaft Diameter. As seen in Fig. 7(*a*), the circulating flow rate is reduced by enlarging the shaft. This is not unexpected because the height and, thus, the cross-sectional area of the flow channel in the tube decrease. The power number, shown in Fig. 7(*b*), remains almost a constant until $d_s/d=0.6$, followed by an increase. It is seen in the figure that the increase in the power number at large shaft diameters is due to the increase in frictional loss ($N^*_{P,f}$). The enlarged shaft causes an increase in the surface velocity and a reduction in the channel height. As a consequence, the shear stress in the channel is increased, which is evidenced in view of the radial variation of circumferential velocity V_θ shown in Fig. 8. Since the shaft surface area also increases with the shaft diameter, the frictional loss is greatly increased at large diameters. The required mixing energy, as shown in Fig. 7(*c*), gradually increases for low values of d_S until $d_S/d=0.6$. It is then followed by a rapid increase.

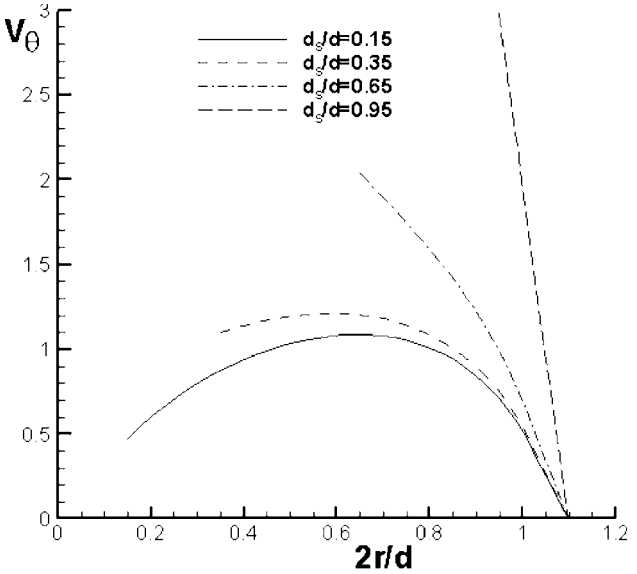

Fig. 8 Distribution of circumferential velocity along the radial direction in the draught tube for different shaft diameters

3.3 Effects of Impeller Pitch. A schematic drawing of the flow channel formed by the impeller blade and the draught tube is deployed onto a plane, as shown in Fig. 9, in which the clearance between the impeller and the tube is neglected. The length of the channel for one revolution of impeller blade is given by $L=S/\sin\alpha$, where α is the helical angle. The flow in the channel can be regarded as being driven by the internal wall of the tube moving in a direction opposite to that of the rotation. This moving wall velocity (V_w) can be divided into two components: one in the channel direction ($V_w \cos\alpha$) and the other in the transverse direc-

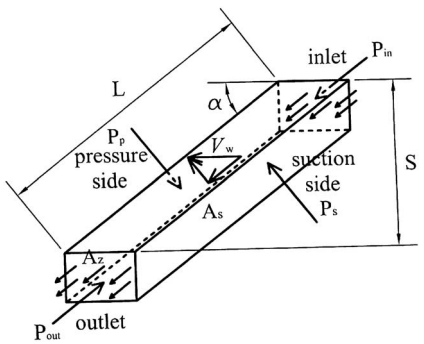

Fig. 9 A schematic drawing of the flow channel inside the draught tube

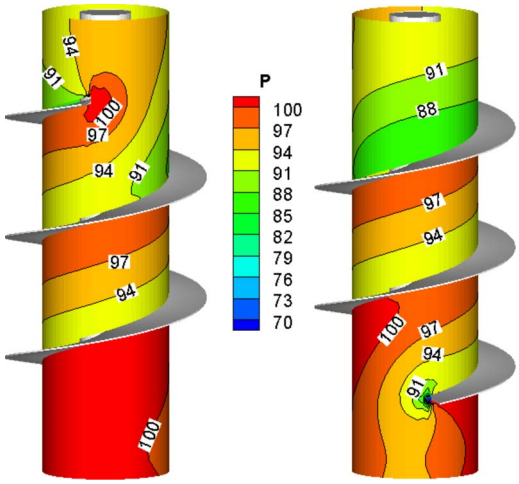

Fig. 10 Pressure distribution on the impeller shaft from two different view angles

tion ($V_w \sin \alpha$). A pressure rise between the inlet and the outlet is built up by the channel-direction flow and a pressure difference between the side walls by the transverse flow. These two pressure differences are related by considering the axial component of the force balance over the entire channel,

$$(p_{\text{out}} - p_{\text{in}})A_z = (p_p - p_s)A_s \cos \alpha - F_z \tag{19}$$

where p_{in} and p_{out} are the pressures at the inlet and the outlet, p_p and p_s are the pressures at the pressure side and the suction side, A_z is the cross-sectional area, A_s is the sidewall area, and F_z is the axial component of the frictional force exerted on the channel walls. In the equation, the momentum difference between the inlet and the outlet is neglected. It is obvious that the pressure difference between the sidewalls is linearly related to the pressure rise through the draught tube. As an illustration, the pressure contours distributed on the impeller shaft are presented in Fig. 10. The dimensionless average pressures at the inlet and exit of the tube are $p_{\text{in}}=91.6$ and $p_{\text{out}}=100.8$, while those on the two sides of the blade are $p_p=104$ and $p_s=87.9$. As a result, the pressure rise through the tube is $p_{\text{in}}-p_{\text{out}}=9.2$ and the pressure difference between the two blade sides is $p_p-p_s=16.1$. It is noted that there exists a high pressure zone at the leading edge of the blade at the entrance and a low pressure zone at the trailing edge at the exit. Near these two regions, reversed flows may result. However, its effect on the primary flow structure is insignificant.

The pitch, or the helical angle α, has two opposite effects on the flow. As seen in Fig. 9, by decreasing the helical angle, the velocity component of the moving wall in the channel direction is increased, being helpful to the fluid flow. However, the channel is narrowed and lengthened, resulting in greater frictional resistance. Hence, there exists an optimum pitch value for maximum flow. It is observed in Fig. 11(*a*) that this optimum value holds at $S/d=1.5$ in the present computations. For the two limiting cases with $\alpha=0$ deg and 90 deg, i.e., $S/d=0$ and ∞, there is no flow through the draught tube because in the former the impeller degenerates into a rotating cylinder, whereas in the latter the impeller blade becomes vertical. For the rotating cylinder case, a large amount of power is required to overcome the great frictional resistance that is prevailing. As shown in Fig. 11(*b*), the power requirement quickly decreases first, followed by leveling off to a constant value. When S is greater than $1.5d$, the constant value of N_P^* is 226 for $S/d=\infty$. It is also shown in the figure that the pressure part of the power number $N_{P,p}^*$ gradually approaches 226 while the frictional part $N_{P,f}^*$ gradually approaches zero. For the limiting case of the vertical blade, transverse flow prevails in the draught tube,

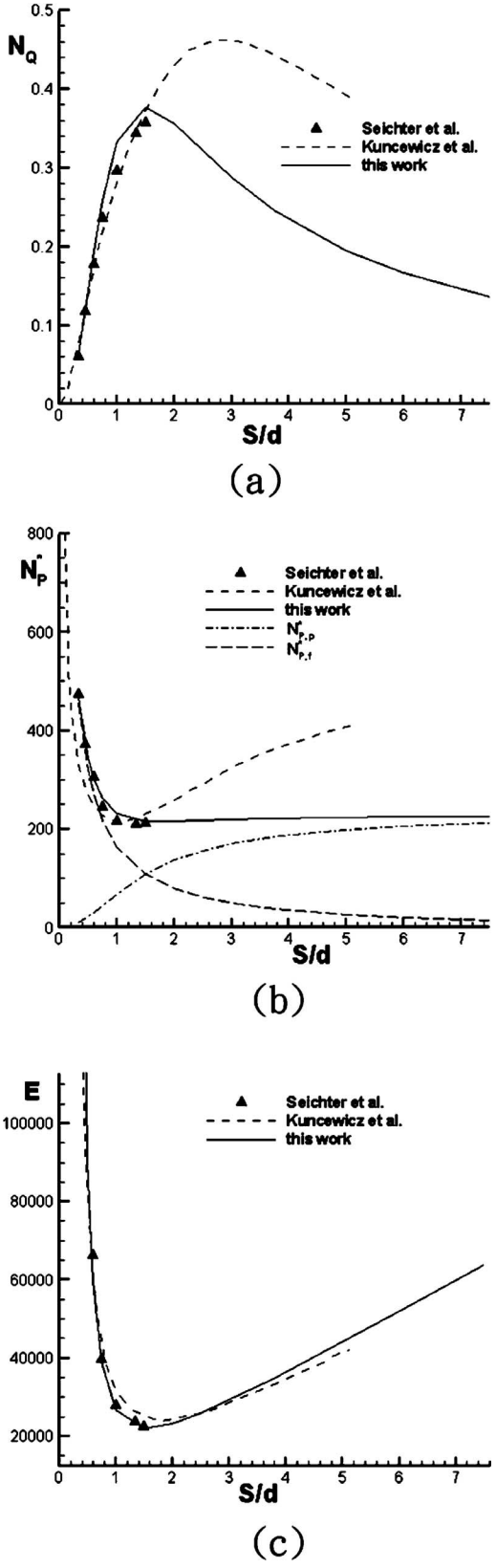

Fig. 11 Variation of (*a*) circulation number, (*b*) power number, and (*c*) mixing energy against screw impeller pitch *S*

which generates large pressure difference between the two sidewalls. The variation of mixing energy in Fig. 11(*c*) shows that the most efficient mixing occurs when $S/d=1.5$.

Compared with the measurements of Seichter et al. [8], the agreement is reasonably good. However, the calculations of Kuncewicz et al. [12] showed that both N_Q and N_P^* are much larger than the present predictions for high values of S. These overpredictions are believed to be due to the drag coefficients used in their model. However, despite the large differences in N_Q and N_P^*, the two calculations yield a close agreement in predicting the mixing energy E.

3.4 Effects of Clearance Gap. It was discussed that a pressure difference is generated between the two sidewalls by the transverse flow, as seen in Fig. 9. The sidewalls represent the two faces of the impeller blade. In practical applications, a passage, i.e., a clearance gap, exists to connect the two sides. Due to the existing pressure gradient, part of the fluid flows through the clearance from the pressure side to the suction side. This flow leakage causes a decrease in the sidewall pressure difference and, in turn, a decrease in pressure rise in the flow channel because they are related, as seen in Eq. (19). Consequently, the circulation number N_Q, the power number N_P^*, and the mixing energy E decrease with increasing clearance C, which are shown in Figs. 12(a)–12(c). It is seen from Fig. 12(b) that the clearance has a significant effect on the frictional force and, thus, the power consumption when the clearance is very small.

3.5 Effects of Draught Tube. A comparison has been made on a system with and without a draught tube by gradually increasing the tank size. It is known that without a tube, a surface vortex may be formed due to the swirling flow generated by the rotating impeller. This surface vortex flow does not exist in the present calculations by assuming that the upper surface is flat. According to Fig. 13(a), the circulation number N_Q for the case without a draught tube is almost linearly related to the tank diameter D in the considered range. For low values of D, the system with a draught tube is superior to that without one. However, it loses superiority when $D>4d$. For the sake of better understanding this result, the mean axial velocity profiles (averaged over the entire circumference) for $D/d=5.0$ at midheight of the tank are shown in Fig. 14. It is seen that by removing the tube, the downward flow induced by the impeller continuously extends to the region far away from the impeller, the point at which the axial velocity $V_z=0$ is the center of the circulation loop. The variation of this circulation center with the tank diameter is shown in Fig. 15. It is evident that the location of this circulation center is nearly proportional to the tank diameter. This explains the previous observation that the flow number N_Q is linearly related to D when the draught tube is not incorporated. It is interesting to notice that for the large tank with $D=5.0d$ shown in Fig. 14, a small amount of induced circulating fluid between the draught tube and the wall of the tank bypasses the tube and flows over the outside surface of the tube. As an illustration of the flow field, the streamlines on a vertical plane for the $D/d=5$ case is prepared in Fig. 16. With the draught tube, there exist small vortices near the inlet and the outlet regions just outside the tube together with the primary circulating loop flow. By removing the tube, the above observed vortices disappear. However, owing to the reduced strength of the downward pumping flow and the enlarged space, a vortex is formed beneath the impeller. It can be seen that without the restriction of the tube, the center of the induced looping flow moves away from the impeller, as discussed in the above.

The power number, shown in Fig. 13(b), is nearly a constant when the tank diameter D becomes greater than $2.5d$. The power consumption is much larger for the case with a draught tube, being about 2.2 times greater than that without a draught tube. This result is supported by the experiments of Chavan et al. [5]. The lower power consumption in the case without a draught tube is mainly ascribed to the large space between the impeller and the wall of the tank, which, in turn, leads to a reduction of pressure gradient and, thus, the power required, as discussed in Sec. 3.4.

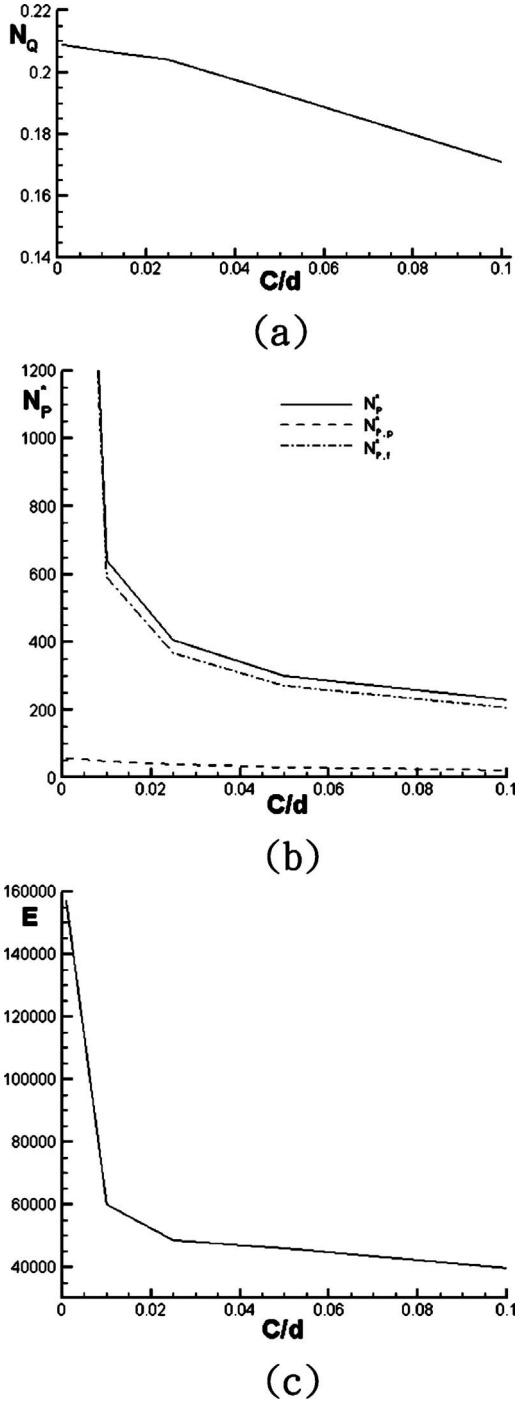

Fig. 12 Variation of (*a*) circulation number, (*b*) power number, and (*c*) mixing energy against clearance *C*

The mixing energy required, shown in Fig. 13(c), for the case with a draught tube is higher than that without a tube. The difference becomes very significant for large tanks.

4 Conclusions

A three-dimensional computational method has been employed to investigate the mixing flow stirred by a screw impeller with a draught tube. The main findings are summarized in the following.

(1) When the tank diameter is slightly greater than that of the draught tube, the narrow passage in the annular space outside the tube restricts the fluid flow and causes large power

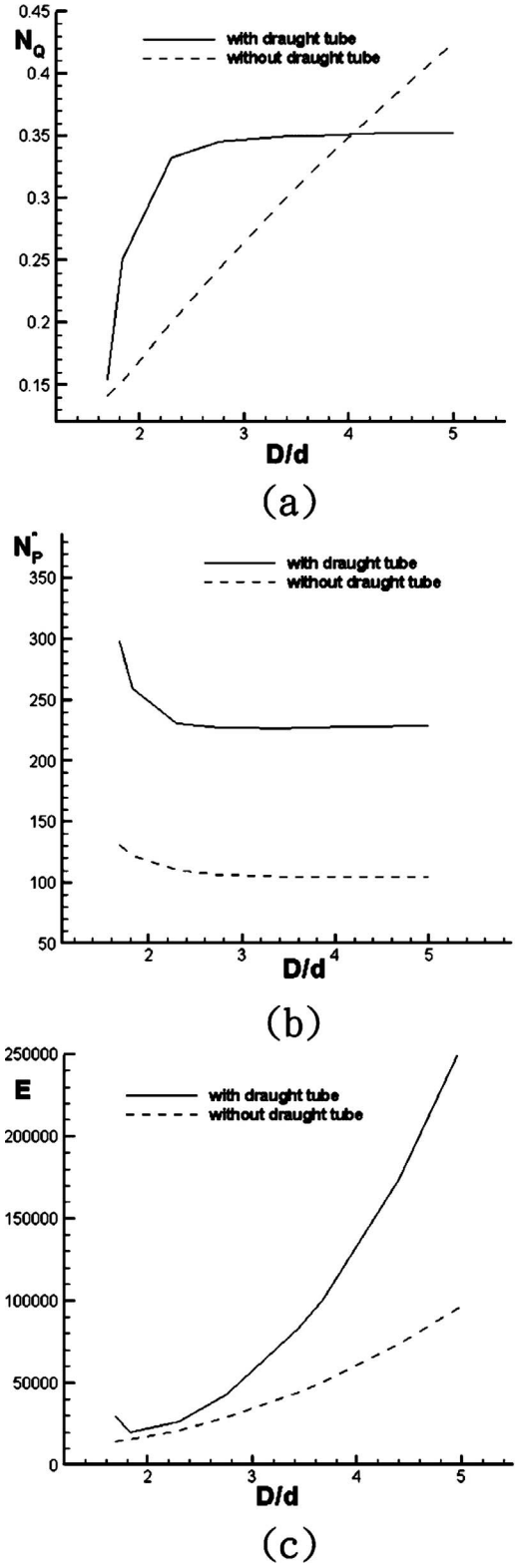

Fig. 13 Variation of (*a*) circulation number, (*b*) power number, and (*c*) mixing energy against tank diameter *D* for the screw impellers with and without a draught tube

consumption. Either the circulation number or the power number nearly reaches a constant for $D > 2.3d$. However, in terms of the total energy required for mixing, the optimum size of the tank occurs at $D=2d$.

(2) The increase in the shaft diameter leads to a decrease in channel height and, thus, reduction in fluid flow. The power requirement remains nearly a constant until $d_s=0.6d$. It is followed by an increase in power consumption due to the enhanced frictional force near the shaft surface.

(3) The flow inside the tube can be considered as a channel

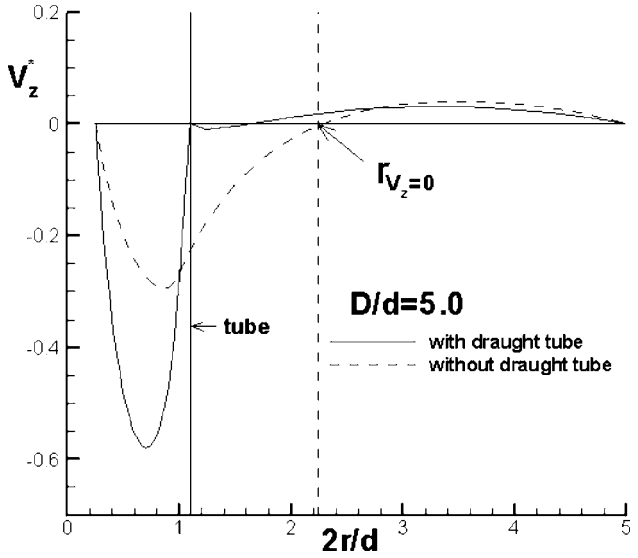

Fig. 14 Distribution of axial velocity along the radial direction for the screw impellers with and without a draught tube

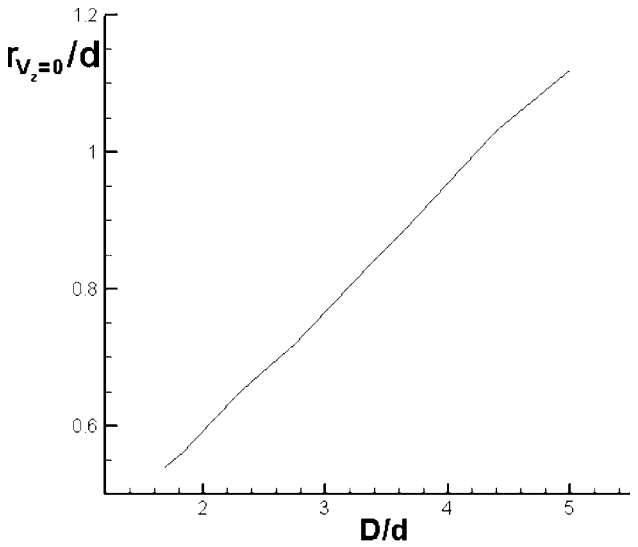

Fig. 15 Variation of circulation center with tank diameter for the case without a draught tube

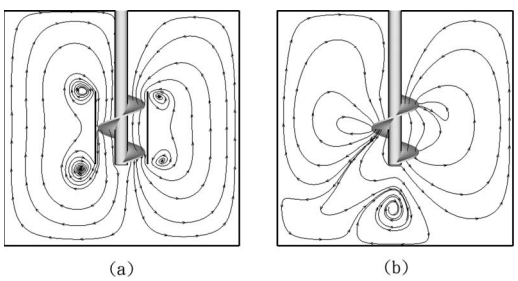

Fig. 16 Flow streamlines on a vertical plane for the screw mixer (*a*) with a draught tube and (*b*) without a draught tube

flow with a moving wall. When the impeller pitch decreases, the velocity component of the moving wall along the channel is increased, but the channel is lengthened and narrowed, resulting in larger frictional resistance. Thus, there exists an optimum value of pitch, which holds at $s/d=1.5$.

(4) The flow leakage from the pressure side to the suction side in the clearance gap brings about a reduction in the pressure difference between the two side surfaces of the impeller blade and, hence, reduces the pressure rise in the tube. As a consequence, both the flow rate and the power requirement decrease.

(5) Without a draught tube, the circulating flow rate is linearly proportional to the size of the tank. Therefore, for sufficiently large tanks, the induced flow rate becomes greater than the system with a draught tube. The linear relationship resulted from the radial movement of the center of the circulating flow. The power requirement for that without a draught tube is about half of that of the system with a draught tube. The lower power required is mainly due to the lower pressure gradients caused by the open space between the impeller and the wall of the tank.

Acknowledgment

This work was supported by the National Science Council of Taiwan, R.O.C. under the Contract No. NSC 96-2221-E-009-135-MY2.

Nomenclature

A_s = sidewall area of pumping channel
A_z = cross-sectional area of pumping channel
C = clearance
d = impeller diameter
d_s = shaft diameter
D = tank diameter
e_j = unit vector in the jth direction of Cartesian coordinates
E = mixing energy $(=\pi(N_p^*/N_Q)(H/D)(D/d)^3)$
f = the faces of the control surface
E_z = axial component of the frictional force exerted on pumping channel walls
h = impeller length
h_1 = distance between the impeller and the top and bottom of the tank
H = liquid height in the tank
L = length of the channel for one revolution of impeller blade
n = rotational frequency of the screw impeller
N_p = power number $(=P/\rho n^3 d^5)$
N_p^* = power number $(=P/\mu n^2 d^3)$
$N_{p,f}^*$ = power number due to frictional force
$N_{p,p}^*$ = power number due to pressure force
N_Q = circulation number $(=Q/nd^3)$
p = pressure
p_{in} = pressure at the inlet of the pumping channel
p_{out} = pressure at the outlet of the pumping channel
p_p = pressure at the pressure side of the pumping channel
p_s = pressure at the suction side of the pumping channel
P = power consumption for a mixing vessel
Q = volumetric flow rate
r = radial distance
Re = Reynolds number $(=\rho nd^2/\mu)$
S = screw pitch
$\mathbf{s}_f$ = surface vector of the considered face
t = thickness of the screw blade
U_{gj} = grid velocity
V_w = moving wall velocity
V_z = axial velocity
V_θ = circumferential velocity
W = blade width

Greek Symbols

α = helical angle of the pumping channel
γ = blending factor
$\vec{\delta}$ = distance vector directed from the upwind node to the centroid of the face
$\vec{\delta}_{PC}$ = distance vector connecting the principal and the neighboring nodes
μ = fluid viscosity
ρ = fluid density
τ_c = circulation time
τ_m = mixing time
Ω_j = angular velocity of the screw impeller

Subscripts

C = neighboring node
f = face value
P = principal node

Superscripts

UD = the value evaluated at a node upstream of the face
$*$ = dimensionless variables

References

[1] Tatterson, G. B., 1991, *Fluid Mixing and Gas Dispersion in Agitated Tanks*, McGraw-Hill, New York.
[2] Paton, J. B., Squires, P. H., Darnell, W. H., Cash, F. M., and Carley, J. F., 1959, "Chap. 4 Extrusion," *Processing of Thermoplastic Materials*, E. C. Bernhardt, ed., Van Nostrand Reinhold, New York.
[3] Carley, J. F., 1962, "Single-Screw Pumps for Polymer Melts," Chem. Eng. Prog., **58**(1), pp. 53–58.
[4] Sykora, S., 1966, "Mixing of Highly Viscous Liquids," Collect. Czech. Chem. Commun., **31**, pp. 2664–2678.
[5] Chavan, V. V., Jhaveri, A. S., and Ulbrecht, J., 1972, "Power Consumption for Mixing of Inelastic Non-Newtonian Fluids by Helical Screw Agitators," Trans. Inst. Chem. Eng., **50**, pp. 147–155.
[6] Chavan, V. V., and Ulbrecht, J., 1973, "Power Correlations for Close-Clearance Helical Impellers in Non-Newtonian Liquids," Ind. Eng. Chem. Process Des. Dev., **12**(4), pp. 472–476.
[7] Chavan, V. V., and Ulbrecht, J., 1973, "Internal Circulation in Vessels Agitated by Screw Impellers," Chem. Eng. J., **6**, pp. 213–223.
[8] Seichter, P., Dohnal, J., and Rieger, F., 1981, "Process Characteristics of Screw Impellers With a Draught Tube for Newtonian Liquids: The Power Input," Collect. Czech. Chem. Commun., **46**, pp. 2007–2020.
[9] Seichter, P., 1981, "Process Characteristics of Screw Impellers with a Draught Tube for Newtonian Liquids: Pumping Capacity of the Impeller," Collect. Czech. Chem. Commun., **46**, pp. 2021–2031.
[10] Seichter, P., 1981, "Process Characteristics of Screw Impellers With a Draught Tube for Newtonian Liquids: Time of Homogenization," Collect. Czech. Chem. Commun., **46**, pp. 2032–2042.
[11] Carreau, P. J., Paris, J., and Guerin, P., 1992, "Mixing of Newtonian and Non-Newtonian Liquids: Screw Agitator and Draft Coil System," Can. J. Chem. Eng., **70**, pp. 1071–1082.
[12] Kuncewicz, C., Szulc, K., and Kurasinski, T., 2005, "Hydrodynamics of the Tank With a Screw Impeller," Chem. Eng. Process., **44**, pp. 766–774.
[13] Kuncewicz, C., and Pietrzykowski, M., 2001, "Hydrodynamic Model of a Mixing Vessel With Pitched-Blade Turbines," Chem. Eng. Sci., **56**, pp. 4659–4672.
[14] Tsui, Y.-Y., and Jung, S.-P., 2006, "Analysis of the Flow in Grooved Pumps With Specified Pressure Boundary Conditions," Vacuum, **81**, pp. 401–410.
[15] Tsui, Y.-Y., Chou, J.-R., and Hu, Y.-C., 2006, "Blade Angle Effects on the Flow in a Tank Agitated by the Pitched-Blade Turbine," ASME J. Fluids Eng., **128**, pp. 774–782.
[16] Tsui, Y.-Y., and Pan, Y.-F., 2006, "A Pressure-Correction Method for Incompressible Flows Using Unstructured Meshes," Numer. Heat Transfer, Part B, **49**, pp. 43–65.